ISSN 0915-633X

NATIONAL INSTITUTE FOR FUSION SCIENCE

Overall Self-Similar Decay of Two-Dimensional Tirbulence

C. Das, S. Kida and S. Goto

(Received - Nov. 13, 2000)

NIFS-672 Dec. 2000

RESEARCH REPORT
NIFS Series

NAGOYA, JAPAN

Overall Self-Similar Decay of Two-Dimensional Turbulence

Chandra DAS, Shigeo KIDA, and Susumu GOTO

Theory and Computer Simulation Center,
National Institute for Fusion Science,
Oroshi-cho 322-6, Toki, 509-5292, Japan

The statistics of two-dimensional decaying turbulence are investigated by the use of direct numerical simulation in a periodic box. A number of cases are systematically compared in which the incompressible Navier-Stokes equation is solved on various resolutions and for various Reynolds numbers starting with random velocity fields of a prescribed energy spectrum. It is observed that the statistics are contaminated rapidly by the periodicity of the flow field which blocks the transfer of velocity fluctuations towards larger scales. At large Reynolds numbers the enstrophy spectrum decays similarly in time throughout the whole wavenumber range and the enstrophy decreases inversely proportionally to time.

KEYWORDS: Self-similar decay, two-dimensional turbulence

1 Introduction

Two-dimensional turbulence has been studied extensively not only for the practical application in geophysics and meteorology to understand and predict the atmospheric and the oceanic flows but also as a simpler model of the three-dimensional counterpart to examine the general properties of turbulence [1, 2]. Indeed the two-dimensional turbulence is less complicated in structure than the three-dimensional one, but the numerical simulation study is not so simple as it looks. Since the modal energy is transferred to larger scales, the characteristic length-scale of the velocity fluctuation ever increases in time. When it grows as large as the simulation domain size, the turbulence statistics, even at small scales, are affected by the boundary condition. The transfer of energy to larger scales is drastically suppressed, for example. Thus, the statistics of turbulence at later times can deviate significantly from those in the infinite domain. This should be kept in mind whenever a long-term numerical simulation is carried out.

As one of the fundamental quantities to describe the turbulence statistics the behavior of the energy spectrum has been investigated in a periodic box by many authors. In order to get the universal behavior independent of initial conditions a long-term numerical simulation is necessary to perform, which brings the possibility of the above-mentioned contamination effects due to the inverse cascade of energy. The k^{-3} power law (with a possible logarithmic correction) of energy spectrum (or the k^{-1} power law of the enstrophy spectrum) in the inertial range derived by the enstrophy cascade theory [3, 4, 5] is not easy to observe in a numerical simula-

tion. Steeper spectra have been frequently reported in literature partly because of the attenuation at large wavenumbers by finite viscosity, and partly because of the accumulation of modal energy around the lowest wavenumbers through the inverse cascade of energy [6, 7]. The formation, the structure, and the distribution of concentrated vortex blobs [8] may also be affected by the simulation domain. These blobs under the periodic boundary condition may lead to the slowdown of the enstrophy decay since the velocity induced by the individual vortices is extremely long-range in two-dimensions. The power p in the algebraic decay law of enstrophy expressed by $\mathcal{Q}(t) \propto t^{-p}$ scatters between 0.3 and 1 [6, 9, 10]. The reason of this wide scatter is not clear.

In the present paper the effects of the simulation domain size on the statistics of the decaying two-dimensional turbulence are systematically investigated. The equations of motion of a two-dimensional incompressible fluid, the scaling properties, and various global statistical quantities are introduced in §2. The numerical method and the parameter setting, the temporal evolutions of the vorticity field and several global quantities are described in §3. A self-similar evolution of the enstrophy spectrum over the whole wavenumber range and the effects of the simulation domain are examined in §4. The concluding remarks are given in §5.

2 Formulation

A decaying two-dimensional motion of an incompressible viscous fluid is described by the vorticity equation, the curl of the Navier-Stokes equation,

$$\frac{\partial \omega}{\partial t} + \frac{\partial}{\partial x_1}(u_1\omega) + \frac{\partial}{\partial x_2}(u_2\omega) = \nu\nabla^2\omega, \quad (1)$$

where

$$\omega(\boldsymbol{x}, t) = \frac{\partial u_2}{\partial x_1} - \frac{\partial u_1}{\partial x_2} \quad (2)$$

is the vorticity. $\boldsymbol{u} = (u_1, u_2)$ is the velocity which satisfies the continuity equation,

$$\frac{\partial u_1}{\partial x_1} + \frac{\partial u_2}{\partial x_2} = 0, \quad (3)$$

$\boldsymbol{x} = (x_1, x_2)$ is the spatial coordinate, and ν is the kinematic viscosity. The velocity field is assumed to be periodic with period 2π both in the x_1 and x_2 directions. The area $(0 \le x_1,\ x_2 \le 2\pi)$ is called the periodic box. Since the governing equations (1)-(3) are invariant under space translations, the periodicity should be preserved if it is imposed at the initial instant.

The energy (per unit mass) of the fluid motion is defined by

$$\mathcal{E}(t) = \frac{1}{2(2\pi)^2}\int |\boldsymbol{u}(\boldsymbol{x}, t)|^2 \mathrm{d}^2\boldsymbol{x}, \quad (4)$$

and the l-th order moment of vorticity by

$$\mathcal{Q}_l(t) = \frac{1}{(2\pi)^2}\int \omega^l(\boldsymbol{x}, t)\mathrm{d}^2\boldsymbol{x}, \quad (5)$$

where l a positive integer, and the integration is carried out over the periodic box. The second-order moment $\mathcal{Q}_2\,(=\mathcal{Q})$ is called the enstrophy. The evolutions of these quantities are described by a hierarchy of equations,

$$\frac{\mathrm{d}\mathcal{E}}{\mathrm{d}t} = -2\nu\mathcal{Q}, \quad (6)$$

$$\frac{\mathrm{d}\mathcal{Q}}{\mathrm{d}t} = -2\nu\mathcal{P}, \quad (7)$$

$$\frac{\mathrm{d}\mathcal{Q}_l}{\mathrm{d}t} = -\nu\frac{l(l-1)}{(2\pi)^2}\int \omega(\boldsymbol{x})^{l-2}[\nabla\omega(\boldsymbol{x})]^2\mathrm{d}^2\boldsymbol{x} \quad (l \ge 2), \quad (8)$$

where

$$\mathcal{P}(t) = \frac{1}{(2\pi)^2}\int (\nabla\omega(\boldsymbol{x}, t))^2\mathrm{d}^2\boldsymbol{x} \quad (9)$$

is the palinstrophy.

Since $\mathcal{Q}$ and $\mathcal{P}$ are positive definite, the right-hand sides of (6) and (7) are negative definite so that $\mathcal{E}$ and $\mathcal{Q}$ always decrease in time. In other words, they are bounded by

their initial values. This implies that the right-hand side of (6) vanishes in the inviscid limit $\nu \to 0$. Recall that $\mathcal{E}$ and all $\mathcal{Q}_l$ $(l \geq 1)$ are constants of motion in the inviscid case $\nu = 0$. In the inviscid limit, however, $\mathcal{Q}$ and $\mathcal{P}$ are supposed to decay sooner or later though $\mathcal{E}$ is a constant of motion. Thus, the two limits, $\nu \to 0$ and $t \to \infty$, are not commutable [11].

Since the flow is periodic, the velocity and vorticity fields can be expanded in the Fourier series as

$$\boldsymbol{u}(\boldsymbol{x}, t) = \sum \check{\boldsymbol{u}}(\boldsymbol{k}, t) \exp[\mathrm{i}\boldsymbol{k} \cdot \boldsymbol{x}], \quad (10)$$

$$\omega(\boldsymbol{x}, t) = \sum \check{\omega}(\boldsymbol{k}, t) \exp[\mathrm{i}\boldsymbol{k} \cdot \boldsymbol{x}], \quad (11)$$

where a check denotes the Fourier coefficient and the summation is taken over all integral vectors $\boldsymbol{k} = (k_1, k_2)$. The energy spectrum may be defined by

$$E(k, t) = \sum_{k \leq |\boldsymbol{k}'| < k+1} \tfrac{1}{2} |\check{\boldsymbol{u}}(k', t)|^2, \quad (12)$$

where $k = 0, 1, 2, \cdots$ are integers. Then, the energy, enstrophy, and palinstrophy are respectively written as

$$\mathcal{E}(t) = \sum_k E(k, t), \quad (13)$$

$$\mathcal{Q}(t) = 2 \sum_k k^2 E(k, t) = \sum_k Q(k, t), \quad (14)$$

$$\mathcal{P}(t) = 2 \sum_k k^4 E(k, t) = \sum_k P(k, t). \quad (15)$$

Here, $Q(k, t) = 2k^2 E(k, t)$ and $P(k, t) = 2k^4 E(k, t)$ are the enstrophy and palinstrophy spectra, respectively.

The equations of fluid motion, (1) and (3), have the following scaling property. Consider two flow fields $\boldsymbol{u}(\boldsymbol{x}, t)$ with viscosity ν and $\boldsymbol{u}'(\boldsymbol{x}', t')$ with viscosity ν' such that

$$\boldsymbol{u}' = \boldsymbol{u}, \quad (16)$$

$$\boldsymbol{x}' = \gamma \boldsymbol{x}, \quad (17)$$

$$t' = \gamma t, \quad (18)$$

$$\nu' = \gamma \nu \quad (19)$$

with a positive constant γ, and therefore,

$$\omega' = \gamma^{-1} \omega. \quad (20)$$

Then, a set of equations (1) and (3) is identical between these two fields. In addition, if their initial conditions are similar,

$$\boldsymbol{u}'(\boldsymbol{x}', 0) = \boldsymbol{u}(\boldsymbol{x}, 0). \quad (21)$$

they will remain so at all the subsequent times,

$$\boldsymbol{u}'(\boldsymbol{x}', t') = \boldsymbol{u}(\boldsymbol{x}, t). \quad (22)$$

Under the scale transformations (16) and (17) the wavenumber and the energy spectrum scale respectively as

$$E'(k', t') = \gamma E(k, t) \quad (23)$$

and

$$k' = \gamma^{-1} k. \quad (24)$$

This scaling property does not hold exactly for the periodic flows unless the period is changed appropriately. Deviations from it, however, are expected to be insignificant for the turbulence statistics if the period is much larger than the characteristic length-scale of turbulence. In the following we examine systematically the effects of periodicity and of numerical resolutions on the statistics of turbulence.

3 Numerical simulation

The initial velocity field is prepared by randomly chosen Fourier coefficients with specified energy spectrum,

$$E(k, 0) = 8\mathcal{E}_0 L_0 (kL_0)^3 \exp\left[-2(kL_0)^2\right], \quad (25)$$

where $\mathcal{E}_0$ is the initial energy and L_0 is the initial large length-scale (see (26) below). The governing equations (1) and (3) are solved numerically by the use of the spectral method for spatial derivatives and the fourth-order Runge-Kutta scheme for time integration. The aliasing errors are

L_0	$N^2 = 1024^2$ ($\nu = 5 \times 10^{-4}$)	$N^2 = 2048^2$ ($\nu = 2.5 \times 10^{-4}$)	$N^2 = 4096^2$ ($\nu = 1.25 \times 10^{-4}$)
$64L_*$	A_1 (392)		
$32L_*$	A_2 (196)	B_1 (392)	
$16L_*$	A_3 (98)	B_2 (196)	C_1 (392)
$8L_*$	A_4 (49)	B_3 (98)	C_2 (196)
$4L_*$	A_5 (24.5)	B_4 (49)	C_3 (98)
$2L_*$		B_5 (24.5)	C_4 (49)
L_*			C_5 (24.5)

Table I. Simulation parameters and symbols of the respective cases. The initial Reynolds numbers Re_0 shown in brackets are common in the cases of the same indices A_n, B_n, C_n ($n = 1, 2, 3, 4, 5$).

removed by the 2/3-rule so that the maximum wavenumber is $N/3$, where N^2 is the number of Fourier modes. Several simulations are performed at various values of initial large length-scale L_0, viscosity ν and resolution N^2 with a prescribed initial energy spectrum (25). The parameters of different cases are summarized in Table I. The symbols A, B, and C represent combined pairs of N^2 and ν. The indices in A, B, and C distinguish different L_0. Here, L_* is a constant ($= 0.0030618\cdots$). The number in brackets after symbols is the initial Reynolds number defined by (31) below. Note that the initial Reynolds number is common between those cases of the same subscripts. Because of the scaling property stated in the preceding section the flows of A_n, B_n, and C_n ($n = 1, 2, \cdots$) are statistically equivalent though different in resolution. These cases may be compared under proper scalings of length and time. The truncation effects at small wavenumbers (or the effects of periodicity) are examined with the effectively same truncation at large wavenumbers by comparing those runs with the same indices, since the ratio of the maximum wavenumber to the peak wavenumber of the initial energy spectrum is common between them.

3.1 Evolution of Vorticity Field

The temporal evolution of vorticity field is shown in Fig.1 for Case C_1. The contour levels are set at integral multiples of the rms of vorticity at each time instant. The regions of positive vorticity are shaded, where fluid elements rotate anti-clockwise. As shown below, since the length-scale increases in proportion to the square-root of time, the size of the displayed domain is increased accordingly. A lot of layers of steep gradients of vorticity are created in the initial stage of evolution (Figs.(b-d)), whereas high-vorticity blobs are more prominent at later times (Figs.(f-h)).

3.2 Decay laws of global quantities

Turbulence is composed of motions of continuously many scales. Among others, those which are dynamically important in decaying turbulence are given by

$$L(t) = \left(\frac{\int_0^\infty E(k,t)\mathrm{d}k}{\int_0^\infty k^2 E(k,t)\mathrm{d}k} \right)^{\frac{1}{2}} = \left(\frac{2\mathcal{E}(t)}{\mathcal{Q}(t)} \right)^{\frac{1}{2}} \tag{26}$$

and

$$l(t) = \left(\frac{\int_0^\infty Q(k,t)\mathrm{d}k}{\int_0^\infty k^2 Q(k,t)\mathrm{d}k} \right)^{\frac{1}{2}} = \left(\frac{\mathcal{Q}(t)}{\mathcal{P}(t)} \right)^{\frac{1}{2}}. \tag{27}$$

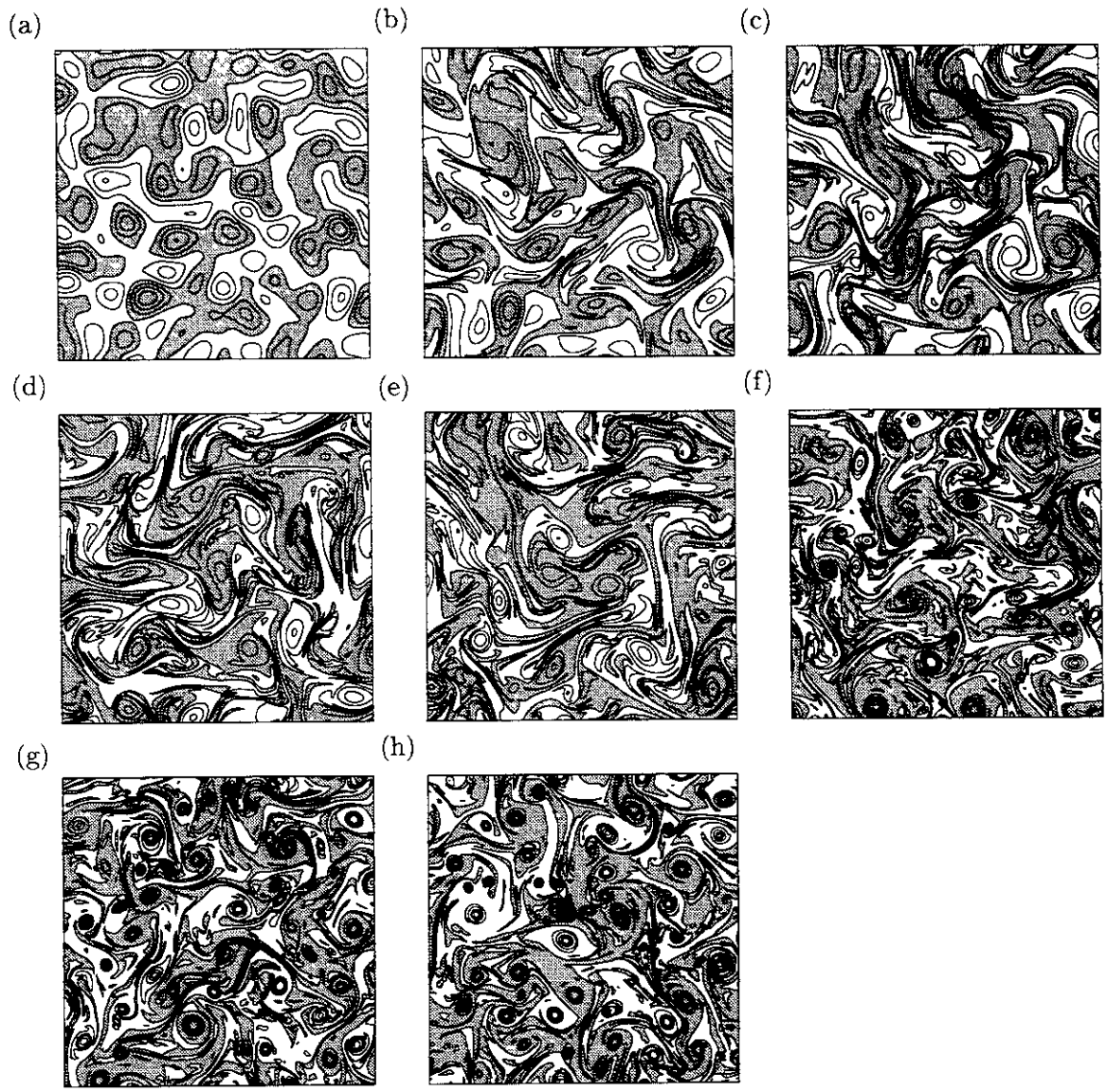

Figure 1: Temporal evolution of vorticity. Case C_1 ($N^2 = 4096^2$). (a) $\tilde{t} = 0$ (the size of displayed domain is 1024^2 in grid number), (b) 2.5 (1024^2), (c) 5 (1024^2), (d) 10 (1024^2), (e) 20 (1448^2), (f) 41 (2048^2), (g) 82 (2896^2), (h) 163 (4096^2). The levels are set at integral multiples of the rms of vorticity at each time instant. Positive regions are shaded.

These are the inverses of the rms wavenumber weighted by the energy and enstrophy spectra, respectively. The energy-averaged length $L(t)$ is called the large length-scale and the enstrophy-averaged length $l(t)$ the small length-scale. For the present initial energy spectrum (25) these two lengths are related as $l_0 = \sqrt{2/3}\ L_0$, where $l_0 = l(0)$ and $L_0 = L(0)$ are the initial values. Hereafter, the length and time are normalized by L_0 and $T_0 = L_0/{\mathcal{E}_0}^{1/2}$ respectively, and a normalized quantity is expressed with a tilde. In Fig.2(a), we plot the temporal evolution of the large length-scale for series C. Lower lines are for larger Reynolds numbers. After the initial constant stage of evolution, it increases algebraically, approximately in proportion to $t^{1/2}$. The period of the initial stage increases with the initial Reynolds number Re_0 $(= Re(0))$ defined by (31) below.

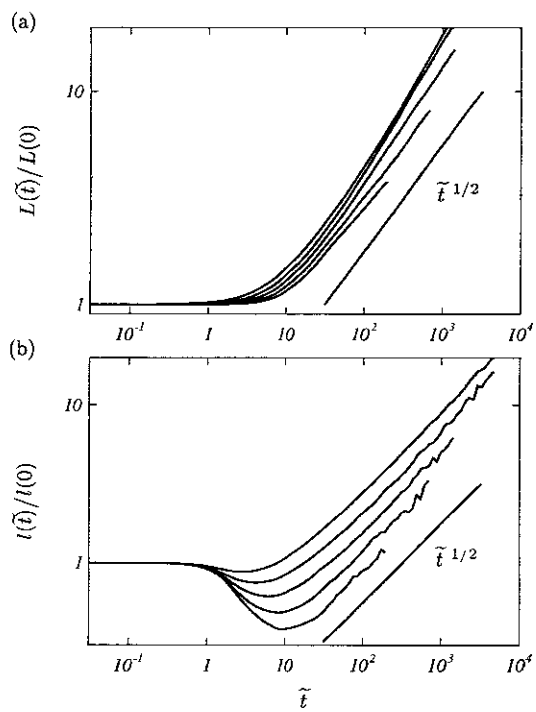

Figure 2: Temporal evolutions of (a) large length-scale L and (b) small length-scale l. The individual curves indicate Cases C_1, C_2, C_3, C_4, C_5 from the bottom.

The temporal evolution of the small length-scale is shown in Fig.2(b). It decreases initially, takes a minimum, and then increases algebraically in time, also in proportion to $t^{1/2}$. The wiggles indicate a sign of the box-size effects. (Variations of comparable order exist in $L(t)$, but the wiggles are invisible in Fig.2(a) because $L(t) \gg l(t)$.) They appear earlier for series A and B (figures not shown) because of less room between the minimum wavenumber and the peak wavenumber of the initial enstrophy spectrum. The first decrease of $\tilde{l}(\tilde{t})$ is due to the enstrophy transfer to larger wavenumbers. For a larger value of the Reynolds number, it takes a smaller minimum at a later time. It is seen from Tables I and II that the minimum value depends on the initial Reynolds number as $\tilde{l}_{\min} \approx 2.3{Re_0}^{-1/3}$, whereas the critical time as $\tilde{t}_{l_{\min}} \approx 1.2{Re_0}^{1/3}$ so that $\tilde{l}_{\min} \approx 2.8\ \tilde{t}_{l_{\min}}^{-1}$. This suggests that a two-dimensional flow may not become singular at a finite time [11, 12, 13]. By equating the above relation of $\tilde{l}_{\min}$ to the initial value $\tilde{l}_0$ $(= \sqrt{2/3})$, we obtain $Re_0 \approx 22$, the Reynolds number which would generate the same small-scales as that of the initial velocity field. In other words, new smaller scales are never exited at the initial Reynolds numbers below 22.

The Reynolds number dependence of the minimum length and the critical time may be understood as follows. The minimum length corresponds to the thickness of the band regions of high-vorticity gradient surrounding high-vorticity blobs in the early stage of evolution (Figs.1(b, c)). For a qualitative understanding, let us consider a Rankine vortex of vorticity distribution,

$$\omega(r,\theta) = \begin{cases} \omega_0 & (r < L_0), \\ 0 & (r > L_0), \end{cases} \qquad (28)$$

which induces the circumferential velocity field as

$$u_\theta(r,\theta) = \begin{cases} \frac{1}{2}\omega_0 r & (r < L_0), \\ \frac{1}{2}\omega_0 {L_0}^2\ r^{-1} & (r > L_0). \end{cases} \qquad (29)$$

Case	$\tilde{l}_{\min}$ (at $\tilde{t}_{l_{\min}}$)	$\Delta\mathcal{P}_{\max}/\mathcal{P}_0$ (at $\tilde{t}_{\mathcal{P}_{\max}}$)	p
C_1	0.31 (at 8.8)	4.4 (at 7.6)	1.01
C_2	0.40 (at 8.1)	2.3 (at 5.5)	1.07
C_3	0.50 (at 5.9)	1.0 (at 4.0)	1.30
C_4	0.61 (at 4.3)	0.4 (at 2.7)	1.49
C_5	0.72 (at 2.9)		1.64

Table II. The shortest small length-scale, the peak palinstrophy, and the power of enstrophy decay for series C.

This vortex deforms a fluid line, which is located on the x-axis at $t = 0$, as $\theta = u_\theta t/r$ at time t in the cylindrical coordinate representation. The shape of the line at t is then expressed as (Fig.3(b))

$$\theta = \begin{cases} \frac{1}{2}\omega_0 t,\ \frac{1}{2}\omega_0 t + \pi & (r < L_0), \\ \frac{1}{2}\omega_0 {L_0}^2 t r^{-2},\ \frac{1}{2}\omega_0 {L_0}^2 t r^{-2} + \pi & (r > L_0). \end{cases} \tag{30}$$

The distance Δr of adjacent fluid lines wrapped around the Rankine vortex is estimated to be $\Delta r = 2\pi r^3/({L_0}^2\omega_0 t) \approx 2\pi L_0/(\omega_0 t)$ near the periphery of the vortex at $\omega_0 t \gg 1$. Now consider the balance of the advection and diffusion of passive vorticity. The advection time, which is estimated by the time-scale of the change of Δr, is $(\mathrm{d}\Delta r/\mathrm{d}t)/\Delta r \approx 1/t$, whereas the viscous diffusion time-scale is $\nu/(\Delta r)^2 \approx \nu{\omega_0}^2 t^2/{L_0}^2$. By equating these two time-scales, we find $t^3 \approx {L_0}^2/(\nu{\omega_0}^2) \approx \mathcal{E}_0/(\nu{\mathcal{Q}_0}^2)$, so that $t \approx {\mathcal{Q}_0}^{-1/2}{Re_0}^{1/3}$ and $\Delta r = L_0 {Re_0}^{-1/3}$. This explains the numerical results shown above. A closure theory suggests that the critical time retards as the Reynolds number increases [14]. It predicts that the critical time is proportional to $(\ln Re_0)^{1/2}$, which is determined as the time when the large-scale disturbances cascade down to the smallest scales of order of $\nu^{1/2}\eta^{-1/6}$, where η is the enstrophy dissipation rate. The discrepancy of this prediction and the present numerical simulation may be attributed to the fact that the flow is not in a state of fully developed turbulence at the initial stage and that the Reynolds number

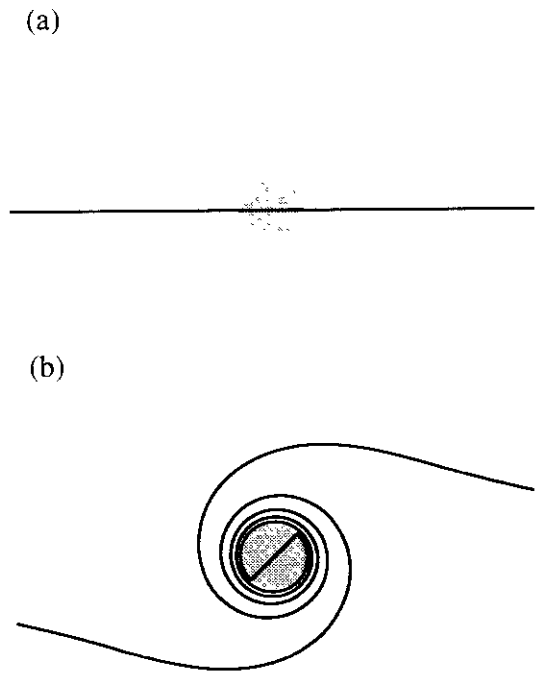

Figure 3: A passive line wrapped by a Rankine vortex. (a) A passive line is placed on the x-axis at the initial time. (b) A Rankine vortex of vorticity ω_0 located at the origin deforms the line into double spirals $r = (\sqrt{21\pi}/2)\theta^{-1/2}$ $(0 < \theta \leq 21\pi/4)$ and $r = (\sqrt{21\pi}/2)(\theta - \pi)^{-1/2}$ $(\pi < \theta \leq 25\pi/4)$ outside the vortex at a later time $t = 21\pi/4\omega_0$. It remains straight inside the vortex of a solid body rotation.

depencence of the smallest scales is different in the two cases.

The relative magnitude of the advection term to the viscous term is measured by the Reynolds number,

$$Re = \frac{UL}{\nu} = \frac{\sqrt{2}\mathcal{E}}{\nu \mathcal{Q}^{1/2}}, \tag{31}$$

where the velocity and length-scales are estimated by $U(t) = \mathcal{E}(t)^{1/2}$ and (26), respectively. Note that Re is not the ratio of $L(t)$ and $l(t)$, the large and small length-scales. (In three-dimensional turbulence, (26) and (27) give respectively the Taylor length-scale and the Kolmogorov length-scale, and the ratio of the two lengths is proportional to a quarter of the Reynolds number.) As will be shown in §4.2, the non-invariance of Re does not exclude the possibility of the overall self-similar evolution of the enstrophy spectrum. The temporal evolution of the Reynolds number is plotted in Fig.4 for all the cases simulated. Here, the solid, dashed, and dotted lines are for the high, intermediate, and low resolutions. It hardly changes in the initial stage and increases algebraically in proportion to $t^{1/2}$ after the critical time $\widetilde{t}_{l_{\min}}$.

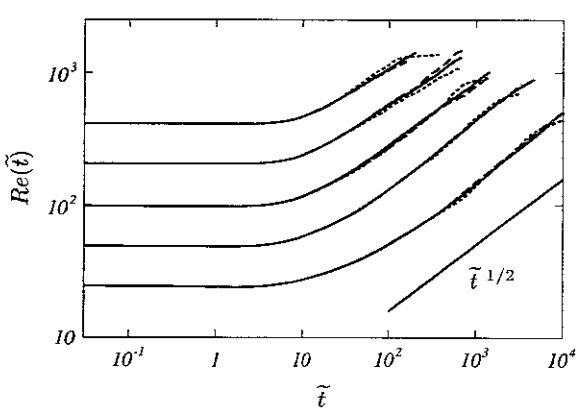

Figure 4: Temporal evolution of the Reynolds number. The solid, dashed, and dotted curves indicate the runs of resolutions 4096^2, 2048^2, and 1024^2, respectively.

The temporal evolutions of the energy, enstrophy, and palinstrophy are plotted in Fig. 5. The meaning of the lines is the same as in Fig.4. Deviations observed at later times between different resolutions are due to contamination effects by the periodicity. Both the energy and enstrophy decrease monotonically in time. As the initial Reynolds number increases, the energy tends to be invariant but the enstrophy never ceases decaying. After the initial constant period, which is also longer for larger Reynolds numbers, the enstrophy decreases algebraically in time as

$$\frac{\mathcal{Q}(t)}{\mathcal{Q}(0)} \propto t^{-p}. \tag{32}$$

The power p seems to go down to unity as the initial Reynolds number increases (see the right-most column in Table II).

The palinstrophy, which is proportional to the time-derivative of the enstrophy (see (7)), increases initially, takes a maximum, then decreases algebraically in time. The maximum value increases in proportion to the initial Reynolds number as

$$\frac{\mathcal{P}_{\max} - \mathcal{P}(0)}{\mathcal{P}(0)} \approx 0.011\ Re_0, \tag{33}$$

and the peak time $\widetilde{t}_{\mathcal{P}_{\max}}$ also increases with the Reynolds number as $\propto {Re_0}^{1/3}$. This Reynolds number dependence of $\mathcal{P}_{\max}$ suggests that the enstrophy dissipation remains nonzero finite in the inviscid limit.

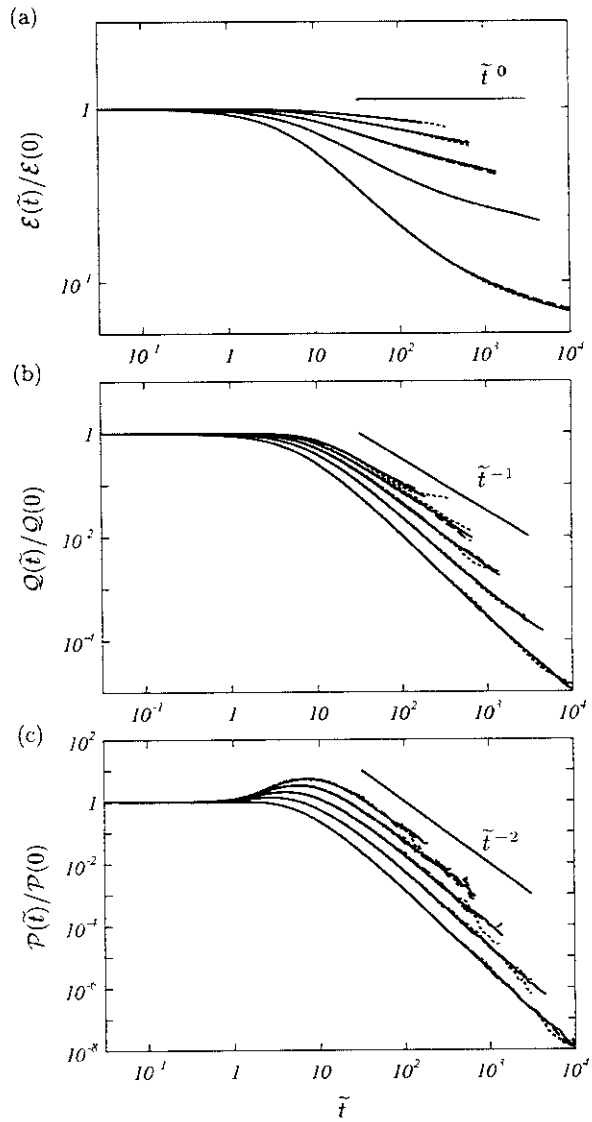

Figure 5: Temporal evolutions of (a) energy, (b) enstrophy, and (c) palinstrophy. Upper curves are for larger Reynolds numbers. The solid, dashed, and dotted curves indicate the runs of resolutions 4096^2, 2048^2, and 1024^2, respectively.

4 Evolution of enstrophy spectrum

4.1 Effects of periodicity

As stated in the introduction, one of the most prominent features of two-dimensional turbulence is the transfer of velocity fluctuations toward larger scales. This is a consequence of the governing equations having two inviscid invariants, i.e. the energy and the enstrophy. This property may cause a severe restriction on the long-term numerical simulation study of the statistics of two-dimensional turbulence. That is, the periodicity may contaminate the statistics sooner or later. Since there is no room below the lowest wavenumber corresponding to the size of the simulation box, the transfer of energy to large-scales is blocked there, which results in an accumulation of the energy so that the energy (and also the enstrophy) spectrum should be deformed substantially from that in the infinite domain [6]. This effect will be examined below.

In Figs.6, we plot the temporal evolution of the enstrophy spectrum for three different initial Reynolds numbers on three different resolutions. Series A_1, B_1, and C_1 are compared in Fig.(a) at eight time instants. The abscissa covers the whole wavenumber range of Case C_1. The three vertical lines on the left side indicate the lower limits of the wavenumber in Cases C_1, B_1, and A_1 in this order from the left. Small deviations in the spectra observed at the initial instant are due to the discreteness of the wavenumber space. As time evolves, the spectrum begins to extend to larger wavenumbers until $\tilde{t} = 7.6$, when the palinstrophy takes the maximum (see Fig.5(c)). After this time, the spectrum decays throughout the whole wavenumber range. Meantime, the top of the spectrum moves left to smaller wavenumbers, which implies the transfer of energy to large scales.

(a)

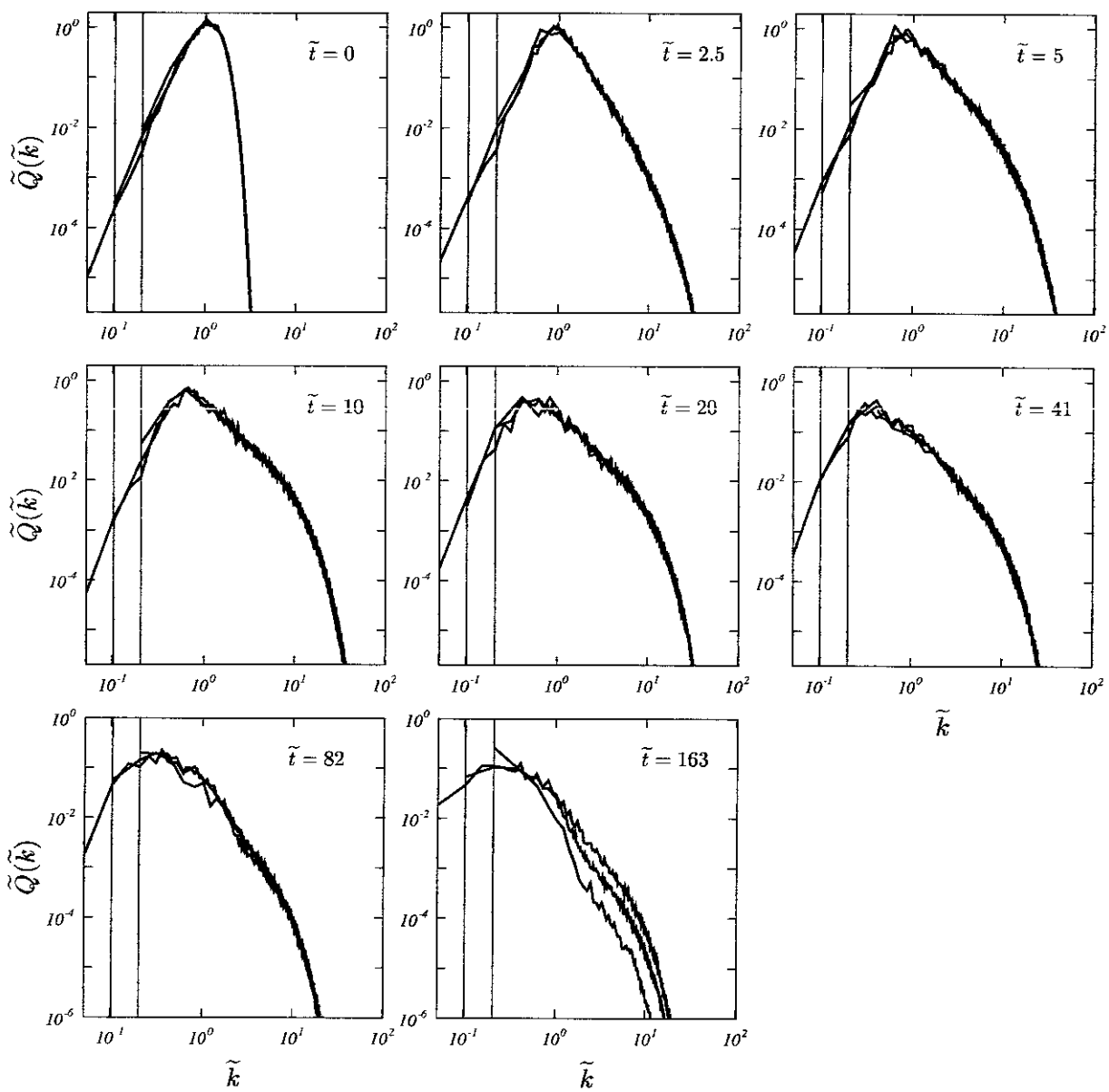
$\widetilde{t} = 0$
$\widetilde{t} = 2.5$
$\widetilde{t} = 5$
$\widetilde{t} = 10$
$\widetilde{t} = 20$
$\widetilde{t} = 41$
$\widetilde{t} = 82$
$\widetilde{t} = 163$
$\widetilde{Q}(\widetilde{k})$
$\widetilde{k}$

(b)

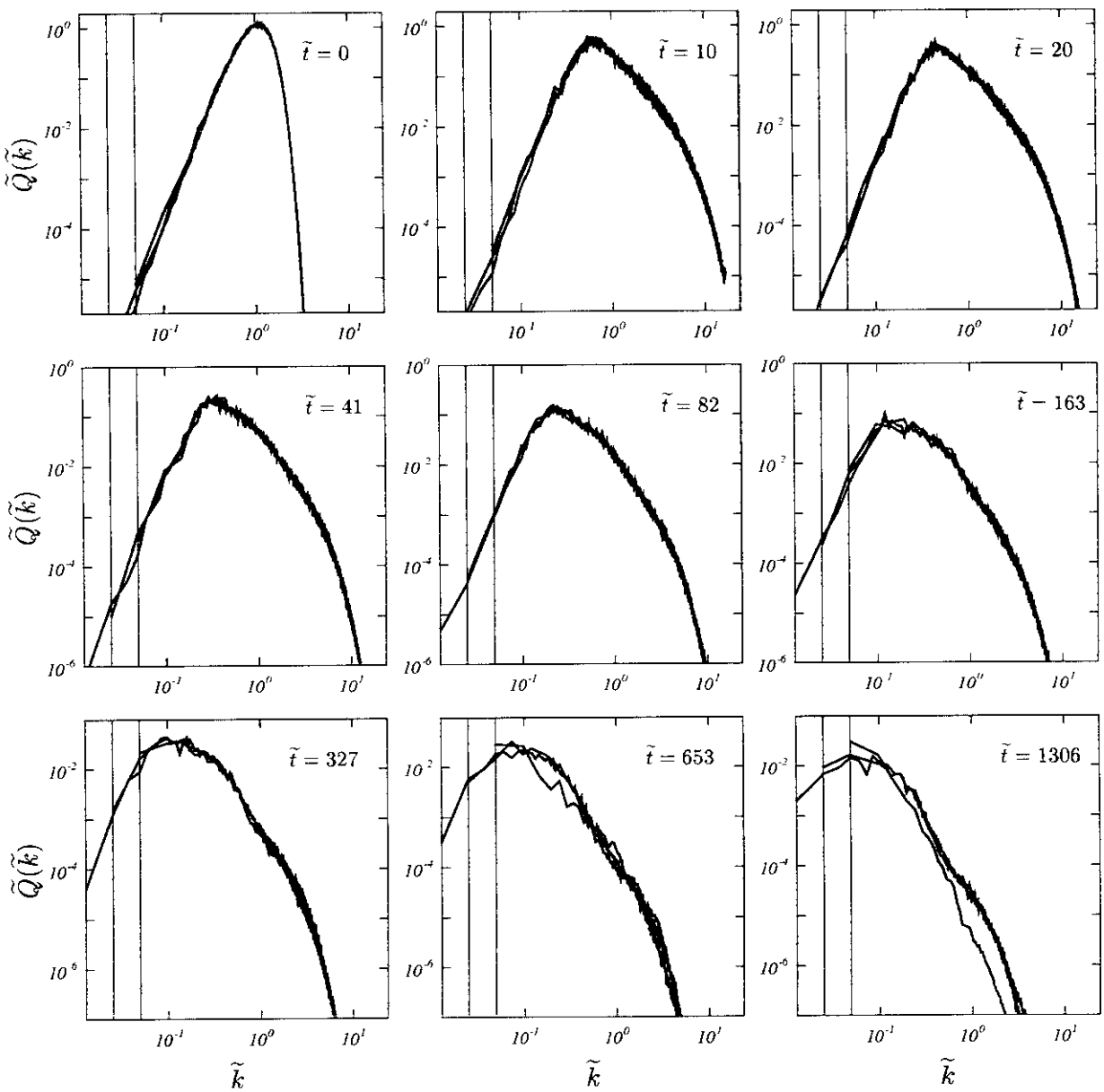
$\widetilde{t} = 0$
$\widetilde{t} = 10$
$\widetilde{t} = 20$
$\widetilde{t} = 41$
$\widetilde{t} = 82$
$\widetilde{t} = 163$
$\widetilde{t} = 327$
$\widetilde{t} = 653$
$\widetilde{t} = 1306$
$\widetilde{Q}(\widetilde{k})$
$\widetilde{k}$

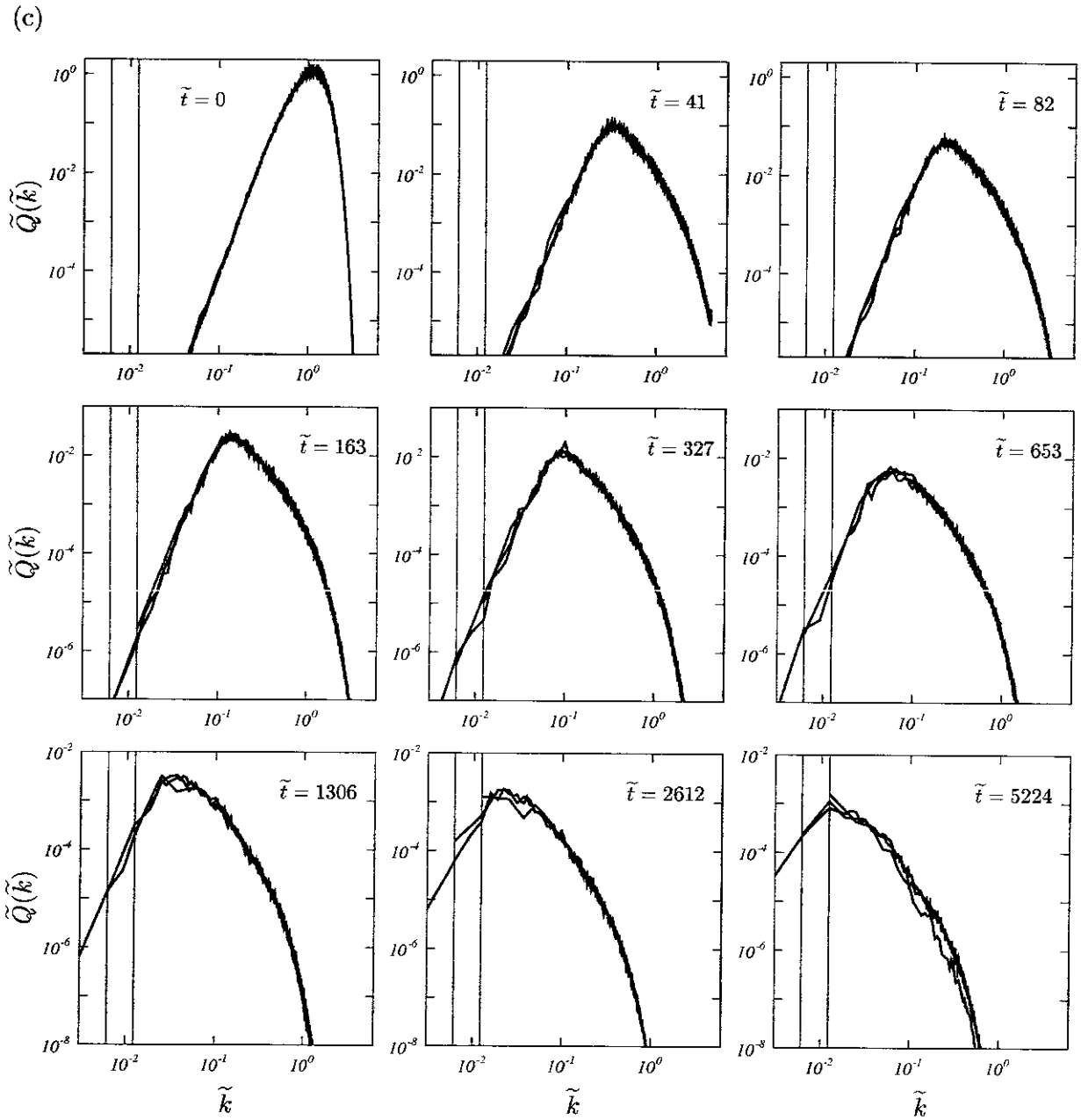

Figure 6: Comparison of temporal evolution of enstrophy spectrum. (a) Cases A_1, B_1, C_1, $Re_0 = 392$, (b) A_3, B_3, C_3, $Re_0 = 98$, (c) A_5, B_5, C_5, $Re_0 = 24.5$. The enstrophy spectrum and the wavenumber are normalized by $\mathcal{E}_0/L_0$ and L_0, respectively. The three vertical lines on the left of each figure denote the minimum wavenumber in Cases A (right), B (middle), and C (left). The spectrum in each case can be distinguished with reference to this lower boundary of the wavenumber. The effects of box-size become substantial when the peak of the spectrum crosses the minimum wavenumber.

The spectrum is prepared at the initial instant in such a way that the enstrophy spectrum starts at small wavenumbers as $Q(k,0) \propto k^5$ (see (25)). This slope seems invariant in time as long as the box-size effects are not significant. This is consistent with the prediction of closure theories [14, 15]. Beyond the spectral peak, on the other hand, the enstrophy spectrum takes the k^{-2} power form over one decade of wavenumbers in the period $5 \leq \tilde{t} \leq 41$. This spectrum is known to be created by line discontinuities in the vorticity field [18, 16, 17], which is consistent with the existence of many convoluted thin layers of high-vorticity gradient in Figs.1 (c)-(f). As time progresses further, the peak of the spectrum approaches the lower bound of the wavenumber and the spectra at different resolutions deviate substantially from each other. Typically the spectrum becomes concave at the intermideate wavenumbers by the boundary effects as the results of the accumulation of energy at the lowest wavenumber (see Figs.6(a), $\tilde{t} \geq 82$ and the last two curves in Fig.7(a)). This is an indication of strong non-local interaction between Fourier modes of different scales. The k^{-1} power law of the enstrophy spectrum derived from the enstrophy cascade theory is not observed by the time when the box-size effects show up. Thus, still higher resolutions are necessary to draw a conclusion whether the k^{-1} power law of enstrophy spectrum is realized or not in a decaying two-dimensional turbulence in the infinite domain. It is interesting to note that concentrated vortex blobs begin to emerge at the same time as the boundary effects do (Figs.1(g)-(h)). It is not clear whether this is merely a coincidence or not.

Figures 6(b) and (c) compare the temporal evolution of the spectrum for series A_3, B_3, C_3 and A_5, B_5, C_5, respectively. The same behavior described above is observed. Here, however, the time of the boundary effects is retarded because the initial spectrum is shifted to larger wavenumbers. No power spectrum is visible on the right-side slope of the top because of the smallness of the Reynolds numbers.

4.2 Overall self-similar evolution of spectrum

The temporal evolution of the enstrophy spectrum for all the five cases of series C is compared in Figs.7. The abscissa covers the whole wavenumber range. The initial peak wavenumber is doubled and the initial Reynolds number is halved successively in the order of (a) to (e). Accordingly, the abscissa is shifted by factor 2 in this order. The effects of the lower bound of the wavenumber starts later in (e) because of larger initial peak wavenumbers, while a closer approach to the high-Reynolds-number asymptotic state is expected in (a) because of higher Reynolds numbers. After the transient period ($\tilde{t} = O(\tilde{t}_{l_{\min}})$), the spectrum enters the self-similar evolution stage in which the shape of the spectrum hardly changes in time in the double logarithmic representation. The effects of the lower boundary of the wavenumber appear as the formation of a dip at the intermediate wavenumbers.

The self-similar evolution is examined by comparing two spectra at different times under a parallel transformation in the double logarithmic representation. The amounts of the shifts in the abscissa and the ordinate give respectively the similarity powers α and β in the form,

$$\tilde{Q}(\tilde{k},\tilde{t}) = t^{\beta} Q^{\dagger}(kt^{\alpha}). \qquad (34)$$

In Fig.8, we compare the spectra at two times $\tilde{t} = 20$ and 41 for Case C_1. The best fit in the sense of the least-square deviations is obtained by shifting the latter horizontally by $\log\Delta\tilde{k} = 1.42$ and vertically by $\log\Delta\tilde{Q} = 1.42$. Then, the powers α and β in (34) are determined to be $\alpha = 0.49$ and $\beta = -0.49$.

If the enstrophy spectrum changes similarly in time as (34), the energy, enstrophy,

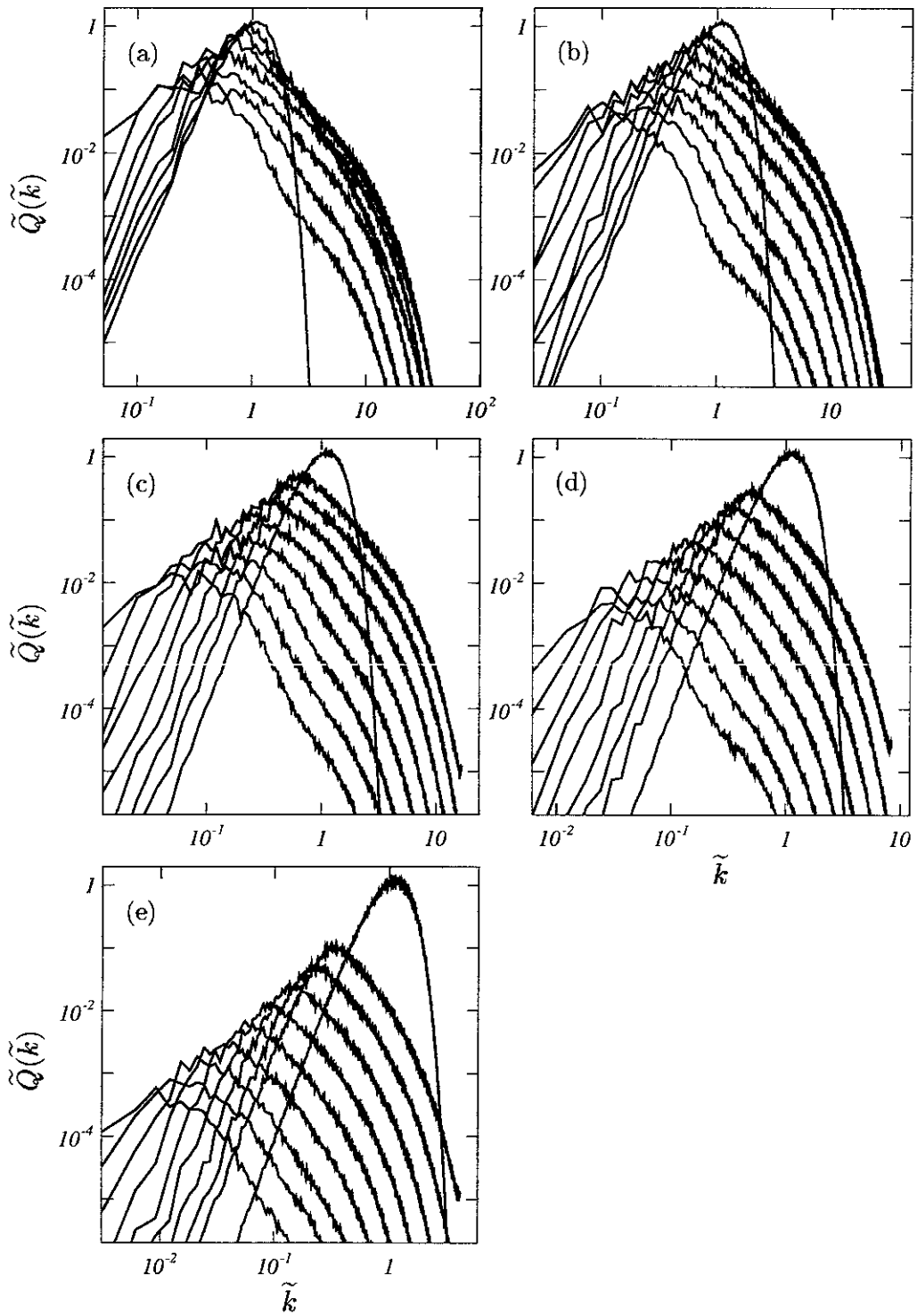

Figure 7: Temporal evolution of enstrophy spectrum. (a) Cases C_1. $Re_0 = 392$. $\widetilde{t} = 0$, 2.5, 5, 10, 20, 41, 82, 163. (b) Cases C_2. $Re_0 = 196$. $\widetilde{t} = 0$, 5, 10, 20, 41, 82, 163, 327, 653. (c) Cases C_3. $Re_0 = 98$. $\widetilde{t} = 0$, 10, 20, 41, 82, 163, 327, 653, 1306. (d) Cases C_4. $Re_0 = 49$. $\widetilde{t} = 0$, 20, 41, 82, 163, 327, 653, f1306, 2612. (e) Cases C_5. $Re_0 = 24.5$. $\widetilde{t} = 0$, 41, 82, 163, 327, 653, 1306, 2612, 5224, 10448. The enstrophy spectrum and the wavenumber are normalized by $\mathcal{E}_0/L_0$ and L_0, respectively. The top of the spectrum goes down as time elapses.

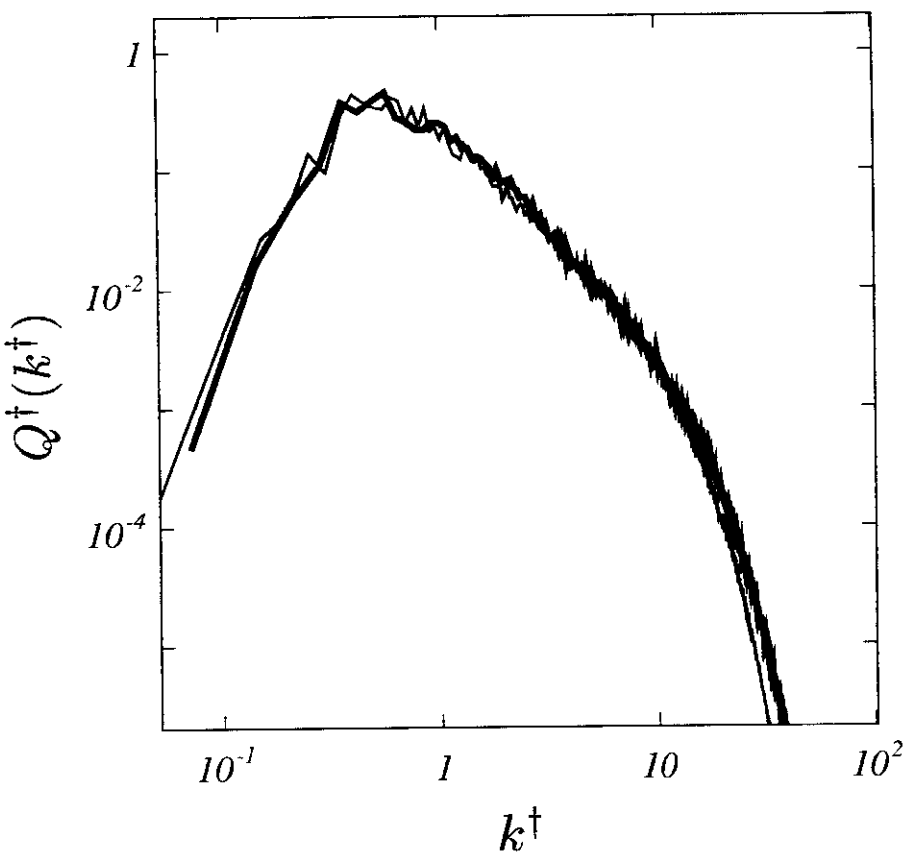

Figure 8: Self-similarity of the enstrophy spectrum. The spectra at $\tilde{t} = 20$ (thin line) and $\tilde{t} = 41$ (thick line) are overlayed by shifting the latter. Case C_1.

and paliostrophy decay algebraically as

$$\mathcal{E}(t) = \tfrac{1}{2}\int_0^\infty k^{-2}t^\beta Q^\dagger(kt^\alpha)\mathrm{d}k$$
$$= \tfrac{1}{2}\,t^{\alpha+\beta}\int_0^\infty k^{\dagger-2}Q^\dagger(k^\dagger)\mathrm{d}k^\dagger, \quad (35)$$
$$\mathcal{Q}(t) = \int_0^\infty t^\beta Q^\dagger(kt^\alpha)\mathrm{d}k$$
$$= t^{-\alpha+\beta}\int_0^\infty Q^\dagger(k^\dagger)\mathrm{d}k^\dagger, \quad (36)$$
$$\mathcal{P}(t) = \int_0^\infty k^2t^\beta Q^\dagger(kt^\alpha)\mathrm{d}k$$
$$= t^{-3\alpha+\beta}\int_0^\infty k^{\dagger2}Q^\dagger(k^\dagger)\mathrm{d}k^\dagger. \quad (37)$$

In the inviscid limit, since the energy is invariant in time, $\mathrm{d}\mathcal{E}/\mathrm{d}t = 0$, we have

$$\alpha = -\beta. \quad (38)$$

The enstrophy equation (7) gives $-\alpha + \beta - 1 = -3\alpha + \beta$, and therefore.

$$\alpha = -\beta = \tfrac{1}{2}, \quad (39)$$

so that

$$L(t) \propto \left(\frac{t}{t_0}\right)^{1/2}, \quad (40)$$

$$l(t) \propto \left(\frac{t}{t_0}\right)^{1/2}, \quad (41)$$

$$\mathcal{Q}(t) \propto \left(\frac{t}{t_0}\right)^{-1}, \quad (42)$$

$$Re(t) \propto \left(\frac{t}{t_0}\right)^{1/2}. \quad (43)$$

These time dependences are consistent with the present numerical results (see Figs.2, 4, and 5). Recently, by a similar numerical study, Chasnov [10, 19] has also obtained the overall self-similar decay of the spectrum and a power law of the enstrophy decay $\mathcal{Q}(t) \propto t^{-p}$ with $p = 0.9$.

5 Concluding Remarks

In spite of apparent simplicity the numerical study of two-dimensional turbulence is not necessarily easier than the three-dimensional one. As a two-dimensional flow evolves, ever larger scales of motions get excited through the inverse cascade process of modal energy and the turbulence statistics are suffered from contamination of simulation domain size as soon as the length-scale becomes comparable with it. This prevents a long-term integration without boundary effects of two-dimensional turbulence and makes it difficult to investigate the statistics of two-dimensional turbulence. In this paper we have investigated how rapidly the effects of numerical domain size arise to contaminate the enstrophy spectrum by comparing many runs systematically which were obtained by solving numerically the two-dimensional Navier-Stokes equation on various resolutions and for various Reynols numbers statring with random velocity fields of a prescribed energy spectrum.

The decay law of the energy spectrum and other statistics have been obtained within a reliable period. When the initial Reynolds number Re_0 is large, the flow dynamics are nearly invsicid in the early stage of evolution until the smallest scales of motions are excited around a time of $O(Re_0)^{1/3}$. Thereafter, the viscous effects come in. the enstrophy spectrum evolves similarly over the whole wavenumber range and the enstrophy decays inversely proportionally to time. The energy-averaged and the enstrophy-averaged lengths as well as the Reynolds number increase in proportion to the square-root of time. It is speculated that the overall self-similar evolution of the enstrophy spectrum is closely related with the strong nonlocal interactions between different scales of motions in the two-dimensional turbulence [15].

The enstrophy spectrum exhibits a power law $Q(k) \propto k^{-q}$ with $q \approx 2$ for quite a long time. However, the celebrated k^{-1} power spectrum based on the enstrophy cascade theory was not observed until the box-size effects arise. The k^{-2} power spectrum is the same as the one predicted by Saffman [18] which is determined by the thin layer

structure of large vorticity gradient. Concerning the evolution of the spectral power, there have been devoted extensive numerical efforts [6, 16, 17], which showed that the k^{-2} power law of the enstrophy spectrum is developed at the early stage of evolution followed by the k^{-1} (with a possible logarithmic correction) spectrum. The latter is understood to be created by much convoluted thin layers of large vorticity gradient. It seems however that the present numerical simulation rings an alarm to this scenario of previous studies because the k^{-1} power spectrum was observed only at later times of evolution when the simulation box-size effects come in.

Another interesting phenomenon which has been observed in the two-dimensional turbulence is the formation of localized strong vortex blobs [8]. There have been lots of discussions on the form of the enstrophy spectrum and the decay law of the enstrophy in terms of vortex blobs [9, 8]. However, we must be careful about the possible effects of the periodicity on the formation of such vortex blobs. As noted in §4.1, many vortex blobs emerge around the time when the boundary effects become important.

A more careful investigation of the box-size effects is necessary for the understanding of the genuine statistics of two-dimensional turbulence.

Acknowledgements

One of the authors, Chandra Das, was supported by COE Research Associateship, Government of Japan, 1998-2000. This work has been partially supported by Grant-in-Aid for Scientific Research on Priority Areas (B) from the Ministry of Education, Science, Sports and Culture of Japan.

References

[1] R.H. Kraichnan & D. Montgomery 1980 Two-dimensional turbulence. Reports Progr. Phys., **43**, 547-619.

[2] R. Moreau (ed.) 1983 *La turbulence bidimensionnelle*, Journal de Mécanique théorique et appliquée (Special issue).

[3] G.K. Batchelor 1969 Computation of the energy spectrum in homogeneous two-dimensional turbulence. Phys. Fluids, **12**, Suppl. II, 233-239.

[4] R.H. Kraichnan 1967 Inertial ranges in two-dimensional turbulence. Phys. Fluids, **10**, 1417-1423.

[5] C.E. Leith 1968 Diffusion approximation for two-dimensional turbulence. Phys. Fluids, **11**, 671-673.

[6] S. Kida, M. Yamada and K. Ohkitani 1988 The energy spectrum in the universal range of two-dimensional turbulence. Fluid Dyn. Res., **4**, 271-301.

[7] T. Gotoh 1998 Energy spectrum in the inertial and dissipation ranges of two-dimensional steady turbulence. Phys. Rev. E, **57**, 2984-2991.

[8] J.C. McWilliams 1990 The vortices of two-dimensional turbulence. J. Fluid Mech., **219**, 361-385.

[9] G.F. Carnevale, J.C. McWilliams, Y. Pomeau, J.B. Weiss & W.R. Yung 1992 Rates, pathways, and end states of nonlinear evolution in decaying two-dimensional turbulence: Scaling theory versus selective decay. Phys. Fluids A **4**, 1314-1316.

[10] J.R. Chasnov 1997 On the decay of two-dimensional homogeneous turbulence. Phys. Fluids, **9**, 171-180.

[11] T. Tatsumi 1980 Theory of homogeneous turbulence. Adv. Appl. Mech., **20**, 39-133.

[12] T. Kato 1967 On classical solutions of the two-dimensional non stationary Euler equation, Arch. Rat. Mech. Analys., **25**, 188-200.

[13] W. Wolibner 1933 Un théorème sur l'existence du mouvement plan d'un fluide parfait, homogène, incompressible, pendant un temps infiniment long. Math. Z., **37**, 698-726.

[14] T. Tatsumi and S. Yanase 1981 The modified cumulant expansion for two-dimensional isotropic turbulence. J. Fluid Mech., **110**, 475-496.

[15] M. Lesieur 1995 *Turbulence in Fluids.* Kluwer.

[16] M.E. Brachet and P.L. Sulem 1985 Free decay of high Reynolds number two dimensional turbulence. Proc. 9th Intern. Conf. on Numerical Methods in Fluid Dynamics, Sacley, Lecture Notes in Physics, **218**, (eds. Soubbramayer and J.P. Boujot (Springer-Verlag, Berlin) pp. 103-108.

[17] S. Kida 1985 Numerical simulation of two-dimensional turbulence with high-symmetry. J. Phys. Soc. Jpn., **54**, 2840-2854.

[18] P.G. Saffman 1971 On the spectrum and decay of random two-dimensional vorticity distributions of large Reynolds number. Stud. Appl. Math., **50**, 377-383.

[19] J.R. Chasnov and J.R. Herring 1999 Self-similar decay of two-dimensional homogeneous turbulence. (preprint).

Recent Issues of NIFS Series

NIFS-657 M Sasao, S Murakami, M Isobe, A V Krasilnikov, S Iiduka, K Itoh, N Nakajima, M Osakabe, K Saito, T Seki, Y Takeiri, T Watari, N Ashikawa, P deVaries, M Emoto, H Funaba, M Goto, K Ida, H Idei, K Ikeda, S Inagaki, N Inoue, S Kado, O Kaneko, K Kawahata, K Khlopenkov, T Kobuchi, A Komori, S Kubo, R Kumazawa, S Masuzaki, T Minami, J Miyazawa, T Morisaki, S Morita, S Muto, T Mutoh, Y Nagayama, Y Nakamura, H Nakanishi, K Narihara, K Nishimura, N Noda, T Notake, Y Liang, S Ohdachi, N Ohyabu, Y Oka, T Ozaki, R O Pavlichenko, B J Peterson, A Sagara, S Sakakibara, R Sakamoto, H Sasao4, K Sato, M Sato, T Shimozuma, M Shoji, H Suzuki, M Takechi, N Tamura, K Tanaka, K Toi, T Tokuzawa, Y Torii, K Tsumori, H Yamada, I Yamada, S Yamaguchi, S Yamamoto, M Yokoyama, Y Yoshimura, K Y Watanabe and O Motojima,
Study of Energetic Ion Transport in the Large Helical Device Sep 2000
(IAEA-CN-77/EX9/1)

NIFS-658 B J Peterson, Y Nakamura, K Yamazaki, N Noda, J Rice, Y Takeiri, M Goto, K Narihara, K Tanaka, K Sato, S Masuzaki, S Sakakibara, K Ida, H Funaba, M Shoji, M Osakabe, M Sato, Yuhong Xu, T Kobuchi, N Ashikawa, P deVries, M Emoto, H Idei, K Ikeda, S Inagaki, N Inoue, M Isobe, S Kado, K Khlopenkov, S Kubo, R Kumazawa, T Minami, J Miyazawa, T Morisaki, S Murakami, S Muto, T Mutoh, Y Nagayama, H Nakanishi, K Nishimura, T Notake, Y Liang, S Ohdachi, Y Oka, T Ozaki, R O Pavlichenko, A Sagara, K Saito, R Sakamoto, H Sasao, M Sasao, T Seki, T Shimozuma, H Suzuki, M Takechi, N Tamura, K Toi, T Tokuzawa, Y Torii, K Tsumori, I Yamada, S Yamaguchi, S Yamamoto, M Yokoyama, Y Yoshimura, K Y Watanabe, T Watari, K Kawahata, O Kaneko, N Ohyabu, H Yamada, A Komori, S Sudo, O Motojima
Impurity transport induced oscillations in LHD Sep 2000
(IAEA-CN-77/EXP5/27)

NIFS-659 T Satow, S Imagawa, N Yanagi, K Takahata, T Mito, S Yamada, H Chikaraishi, A Nishimura, I Ohtake, Y Nakamura, S Satoh, O Motojima,
Achieved Capability of the Superconducting Magnet system for the Large Helical Device Sep 2000
(IAEA-CN-77/FTP1/15)

NIFS-660 T Watari, T Mutoh, R Kumazawa, T Seki, K Saito, Y Torii, Y P Zhao, D Hartmann, H Idei, S Kubo, K Ohkubo, M Sato, T Shimozuma, Y Yoshimura, K Ikeda, O Kaneko, Y Oka, M Osakabe, Y Takeiri, K Tsumori, N Ashikawa, P C deVries, M Emoto, A Fukuyama, H Funaba, M Goto, K Ida, S Inagaki, N Inoue, M Isobe, K Itoh, S Kado, K Kawahata, T Kobuchi, K Khlopenkov, A Komori, A Krasilnikov, Y Liang, S Masuzaki, K Matsuoka, T Minami, J Miyazawa, T Morisaki, S Morita, S Murakami, S Muto, Y Nagayama, Y Nakamura, H Nakanishi, K Narihara, K Nishimura, N Noda, A. TNotake, S Ohdachi, N Ohyabu, H Okada, M Okamoto, T Ozaki, R O Pavlichenko, B J Peterson, A Sagara, S Sakakibara, R Sakamoto, H Sasao, M Sasao, K Sato, S Satoh, T Satow, M Shoji, S Sudo, H Suzuki, M Takechi, N Tamura, S Tanahashi, K Tanaka, K Toi, T Tokuzawa, K Y Watanabe, T Watanabe, H. Yamada, I Yamada, S Yamaguchi, S Yamamoto, K Yamazaki, M Yokoyama, Y Hamada, O Motojima, M Fujiwara,
The Performance of ICRF Heated Plasmas in LHD Sep 2000
(IAEA-CN-77/EX8/4)

NIFS-661 K Yamazaki, K Y Watanabe, A Sagara, H Yamada, S Sakakibara, K Narihara, K Tanaka, M Osakabe, K Nishimura, O Motojima, M Fujiwara, the LHD Group
Helical Reactor Design Studies Based on New Confinement Scalings Sep. 2000
(IAEA-CN-77/ FTP 2/12)

NIFS-662 T Hayashi, N Mizuguchi, H Miura and T Sato
Dynamics of Relaxation Phenomena in Spherical Tokamak Sep 2000
(IAEA-CN-77THP2/13)

NIFS-663 H Nakamura and T Sato, H Kambe and K Sawada and T Saiki,
Design and Optimization of Tapered Structure of Near-field Fiber Probe Based on FDTD Simulation Oct 2000

NIFS-664 N Nakajima,
Three Dimensional Ideal MHD Stability Analysis in $L=2$ Heliotron Systems Oct 2000

NIFS-665 S Fujiwara and T Sato,
Structure Formation of a Single Polymer Chain I Growth of trans Domains Nov 2000

NIFS-666 S Kida
Vortical Structure of Turbulence Nov 2000

NIFS-667 H Nakamura, S Fujiwara and T Sato,
Rigidity of Orientationally Ordered Domains of Short Chain Molecules Nov 2000

NIFS-668 T Mutoh, R Kumazawa T Seki, K Saito, Y Torii F Shimpo, G Nomura, T Watari, D A Hartmann, M Yokota, K Akaishi, N Ashikawa, P deVries, M Emoto, H Funaba, M Goto, K Ida, H Idei, K Ikeda, S. Inagaki, N Inoue, M Isobe, O Kaneko, K Kawahata, A Komori, T Kobuchi, S Kubo, S Masuzaki, T Morisaki, S Morita, J Miyazawa, S Murakami, T Minami, S Muto, Y Nagayama, Y Nakamura, H Nakanishi, K Narihara, N Noda, K Nishimura, K Ohkubo, N Ohyabu, S Ohdachi, Y Oka, M Osakabe, T Ozaki, B.J Peterson, A Sagara, N Sato, S Sakakibara, R Sakamoto, H Sasao, M Sasao, M Sato, T Shimozuma, M Shoji, S Sudo, H Suzuki, Y Takeiri, K Tanaka, K Toi, T Tokuzawa, K Tsumori, K Y Watanabe, I Watanabe, H Yamada, I Yamada, S Yamaguchi, K Yamazaki, M Yokoyama, Y Yoshimura, Y Hamada, O Motojima M Fujiwara,
Fast- and Slow-Wave Heating of Ion Cyclotron Range of Frequencies in the Large Helical Device Nov 2000

NIFS-669 K Mima, M S Jovanovic, Y Sentoku, Z-M Sheng, M M Skoric and T Sato,
Stimulated Photon Cascade and Condensate in Relativistic Laser-plasma Interaction Nov 2000

NIFS-670 L Hadzievski, M M Skoric and T Sato,
On Origin and Dynamics of the Discrete NLS Equation Nov 2000

NIFS-671 K Ohkubo, S Kubo H Idei, T Shimozuma, Y Yoshimura, F Leuterer, M. Sato and Y Takita,
Analysis of Oversized Sliding Waveguide by Mode Matching and Multi-Mode Network Theory Dec 2000

NIFS-672 C Das, S Kida and S Goto,
Overall Self-Similar Decay of Two-Dimensional Tirbulence Dec 2000